MATERIALS CHEMISTRY FRONTIERS

RESEARCH ARTICLE

View Article Online
View Journal | View Issue

Cite this: *Mater. Chem. Front.*, 2022, **6**, 71

Stable two-dimensional lead iodide hybrid materials for light detection and broadband photoluminescence†

Mohamed Saber Lassoued,[ab] Yuan-Chao Pang,[ab] Qian-Wen Li,[ab] Xinkai Ding,[b] Bo Jiao,[cd] Hua Dong,[cd] Guijiang Zhou,[a] Shujiang Ding,[a] Zhicheng Zhang,[a] Zhaoxin Wu,[cd] Gaoyang Gou,*[b] Zongyou Yin,[e] Ju Li[e] and Yan-Zhen Zheng*[ab]

Received 9th September 2021,
Accepted 8th November 2021

DOI: 10.1039/d1qm01247a

rsc.li/frontiers-materials

Two-dimensional (2D) organic–inorganic hybrid materials have attracted widespread attention for photodetection. Moreover, such materials with broadband photoluminescence and strong photocurrent response are still rare. Here, we report two new semiconducting 2D organic–inorganic hybrid materials, namely $\{Pb^{II}_2I_6[Pb^{II}(TETA)]\}_n$ (**1Pb**) and $\{Pb^{II}_3I_8[Pb^{II}(TETA)]\}_n$ (**2Pb**), where TETA = triethylenetetramine, with broadband yellow-green emission. Both compounds are soluble in DMF and yield high surface coverage films through spin coating. Strikingly, the photocurrent responses of such thin films show *ca.* 600 and 700 nA cm^{-2} difference between I_{light} and I_{dark} for **1Pb** and **2Pb**, respectively. To the best of our knowledge, **1Pb** and **2Pb** showed among the highest current obtained in 2D lead iodide hybrid materials under a low voltage (0.7 V). Moreover, **1Pb** and **2Pb** are stable under heat, moisture and light, which may provide realistic applications for light detection.

In recent years, methyl ammonium lead halide materials have become a new path in the photovoltaic field due to their simple manufacturing processes,[1] high absorption coefficient[2,3] and long charge carrier diffusion lengths.[4,5] The interest around these compounds is driven by their fast advancement of the energy conversion efficiency (PCE). Since Miyasaka manufactured the initial device in 2009, its efficiency was 3.8%, and the PCE of organic–inorganic solar cells have been increased to 25.5% in such a short period of time,[6] surpassing the most advanced copper indium gallium diselenide (CIGS) solar cells, and approaching single crystal silicon solar cells.[7] However, under environmental conditions (moisture, oxygen and UV radiation), their stability is still poor and remains a principal drawback for further commercial use.[8–10]

In order to address the long-term stability issue for real-world applications, two-dimensional (2D) hybrid materials have become the best candidates due to their superior stability and wider structural diversity.[11–13] In addition, 2D organic–inorganic hybrid materials also present exciting optical and unique optoelectronic properties, such as widely tunable bandgap energy, extremely large exciton binding energy, layered characteristic and long decay times.[14–18] All these features make those kind of hybrid materials very promising in optoelectronic devices. In particular, 2D lead halide hybrid compounds have been paid extensive attention not only due to their rich structural chemistry (by using different organic cations, a large number of 2D halo-plumbate anions have been investigated such as $[PbX_4]^{2-}$, $[Pb_3X_9]^{3-}$, $[Pb_5X_{14}]^{4-}$, and $[Pb_7X_{18}]^{4-}$)[19–23] but also because of their interesting stability and photophysical properties. In this context, Dou *et al.* synthesized stable 2D hybrid perovskite quantum wells $(4Tm)_2PbI_4$ and $(BTm)_2PbI_4$ using hydrophobic organic semiconducting ligands (4Tm and BTm: thiophene derivatives). Those two compounds showed high stability under harsh conditions (heat and moisture).[24] The employment of larger organic cations with strong π–π interactions within a 2D

[a] *School of Chemistry, Xi'an Key Laboratory of Sustainable Energy and Materials Chemistry, MOE Key Laboratory for Nonequilibrium Synthesis and Modulation of Condensed Matter, Xi'an Jiaotong University, Xi'an 710049, China. E-mail: zheng.yanzhen@xjtu.edu.cn*
[b] *Frontier Institute of Science and Technology (FIST), State Key Laboratory for Mechanical Behavior of Materials, and School of Physics, Xi'an Jiaotong University, Xi'an 710054, China. E-mail: gougaoyang@xjtu.edu.cn*
[c] *Key Laboratory of Photonics Technology for Information, Key Laboratory for Physical Electronics and Devices of the Ministry of Education, Department of Electronic Science and Technology, School of Electronic and Information Engineering, Xi'an Jiaotong University, Xi'an 710049, China*
[d] *Collaborative Innovation Center of Extreme Optics, Shanxi University, Taiyuan 030006, China*
[e] *Department of Nuclear Science and Engineering, Department of Materials Science and Engineering, Massachu-setts Institute of Technology, Cambridge, MA 02139, USA*

† Electronic supplementary information (ESI) available. CCDC [2107024, 2107027]. For ESI and crystallographic data in CIF or other electronic format see DOI: 10.1039/d1qm01247a

structure will greatly enhance the stability of these compounds.[25] Moreover, due to the strong van der Waals interactions between the layers, Li *et al.* showed that 2D Dion Jacobson lead iodide hybrid perovskite $(PA)_2(MA)_3Pb_4I_{13}$ and $(PDA)(MA)_3Pb_4I_{13}$ (PA = propylamine and PDA = 1,3-propanediamine) exhibited ultrahigh stability for 4000 h under 40–70% relative humidity and for 168 h damp heat at 85 °C.[26] Other than that, 2D lead halide hybrid compounds were reported to have excellent luminescence properties; for example, Liu *et al.*[27] prepared two 2D organic–inorganic lead bromide hybrid materials $(C_7H_{18}N_2)PbBr_4$ and $(C_9H_{22}N_2)PbBr_4$, exhibiting broadband emission with a long-life time emission of $\simeq$1 ms; Luo *et al.* also successfully designed a new 2D lead bromide hybrid, (γ-methoxy propyl amine)$_2PbBr_4$, which exhibits bright bluish white light emission with high Color Rendering Index and PLQE of 6.85%;[28] and $[DMEDA]PbCl_4$ (DMEDA = *N*,*N*-dimethylethylenediamine), $(C_6H_5C_2H_4NH_3)_2PbCl_4$, $[DMPDA]PbCl_4$ (DMPDA = *N*,*N*-dimethyl-1,3-diaminopropane), $[(CH_3)_4N]_4Pb_3Cl_{10}$ and $(C_4H_9NH_3)2PbCl_4$ have also been reported as luminescent materials.[29–32]

On the other hand, despite a few literature reports based on 2D lead halide hybrid photodetectors (particularly for 2D lead iodide hybrids), those works showed very interesting and promising results. For example, a 2D bilayered lead iodide hybrid compound reported by Zhang *et al.* exhibited broadband photoresponsive properties with high photoresponsivity.[33] Another important work reported by Huang *et al.* showed a photodetector with tunable photoresponse by the precise control of the n number of 2D $(BA)_2(MA)_{n-1}Pb_nI_{3n+1}$ (n = 1, 2, 3) hybrid materials.[34] Nevertheless, how to realize stable 2D lead iodide hybrid compounds broadband photoluminescence together with strong photo-response is still a huge challenge and very rarely reported.

In light of this discussion, we report two new 2D lead iodide organic–inorganic hybrid materials, namely $\{Pb^{II}{}_2I_6[Pb^{II}(TETA)]\}_n$ (**1Pb**) and $\{Pb^{II}{}_3I_8[Pb^{II}(TETA)]\}_n$ (**2Pb**), which possessed excellent semiconductor properties and broadband yellow-green light emission. In addition to the high solubility and film processable nature, **1Pb** and **2Pb** showed significant stability against moisture, light and temperature, which made **1Pb** and **2Pb** suitable for light detection applications.

1Pb and **2Pb** were synthesized through the hydrothermal technique, in which different stoichiometric amounts of $Pb(NO_3)_2$, triethylenetetramine (TETA) and KI in a concentrated hydroiodic acid (HI) were added, and the mixture was kept for 24 h at 130 °C for **1Pb**, and at 150 °C for 48 h for **2Pb** (see "Materials and sample preparation" in the ESI† for more details). Structural analyses disclosed that **1Pb** crystallized in a monoclinic system with a centrosymmetric space group of $P2_1/c$ at 298 K (Table S1, ESI†). The asymmetric unit comprises one organic triethylenetetramine (TETA), three lead(II) ions and six iodine anions (Fig. 1a).

As shown in Fig. 1b and c, the topography of **1Pb** can be described as a 2D structure, in which there are two crystallographically independent Pb(II) atoms, which exhibited two different coordination environments: $[PbI_6]$ octahedra for both Pb1 and Pb2, while $[PbN_4I_2]$ octahedron for Pb3. Thus, for Pb1

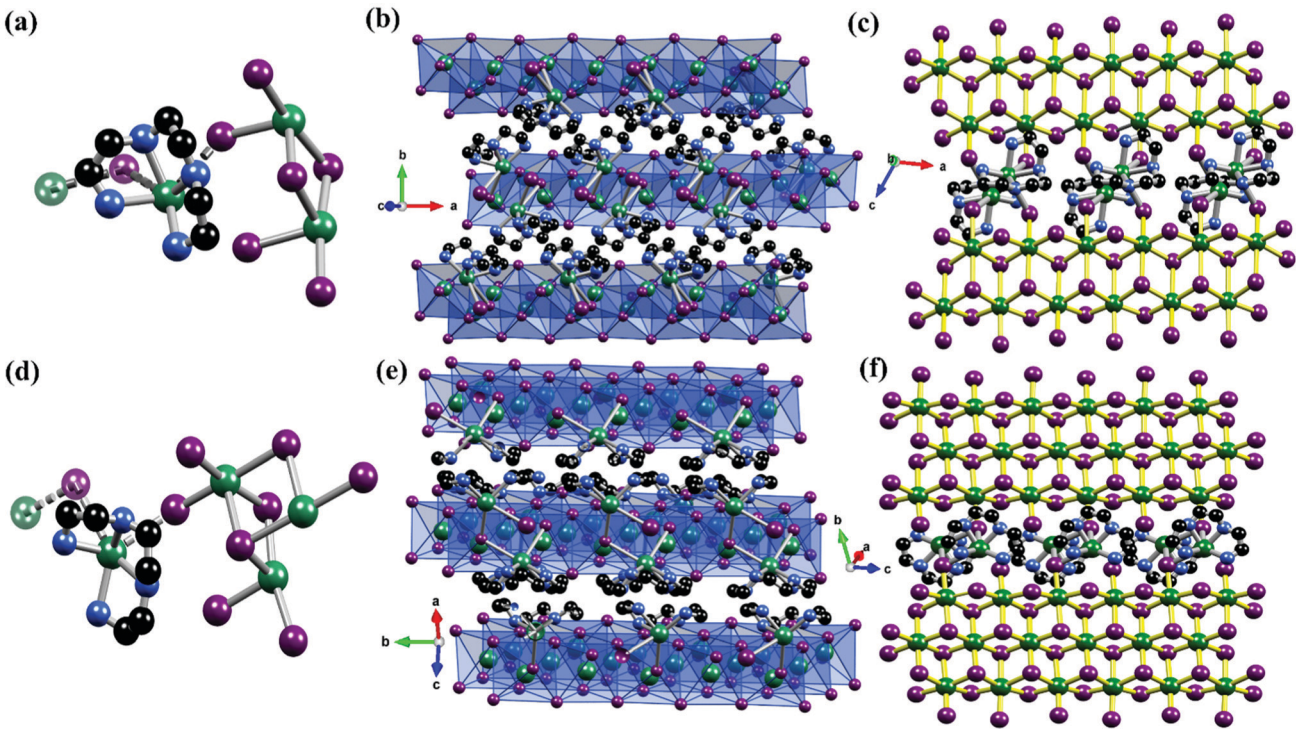

Fig. 1 Asymmetric units of **1Pb** (a) and **2Pb** (d). Crystal structure of the compounds of **1Pb** (b) and **2Pb** (e). Zoom of **1Pb** layer (c) and **2Pb** layer (f). Hydrogen atoms are omitted for clarifications. The colors are used to indicate the following: Lead: dark green, iodine: violet, carbon: black and nitrogen: blue.

and Pb2, each lead atom was connected with six iodine atoms to form PbI_6 octahedra, in that Pb1 and Pb2 were linked together by two bridge I atoms. The Pb–I distances varied between 3.0447 (13) Å and 3.3673 (12) Å, while the I_{eq}–Pb–I_{eq} (“eq” refers to equatorial) bond angles ranged from 80.41 (3)° to 105.96 (3)°, and the I_{ax}–Pb–I_{ax} (“ax” refers to axial) bond angles varied between 162.51 (3)° and 177.28 (4)°, indicating that the octahedra were distorted. The Pb3 atom was bonded to four N atoms and shared two iodine atoms with $[Pb_2I_6]$ units to form $[PbN_4I_2]$ octahedron, in which the Pb–I bond lengths varied between 3.5192 (13) Å and 3.662 (16) Å; the Pb–N distance ranged from 2.4470 (15) Å to 2.628 (17) Å and the N–Pb–N angle ranged from 68.6 (6)° to 122.4 (6)° (Table S2, ESI†). Hence, a 2D $\{Pb^{II}{}_2I_6[Pb^{II}(TETA)]\}_n$ network was formed by sharing two iodine atoms between the $[Pb_2I_6]^{2-}$ and $[Pb(TETA)]^{2+}$ units.

Using different stoichiometric amounts from **1Pb**, yellow crystals of **2Pb** were synthesized. Single-crystal X-ray diffraction studies revealed that **2Pb** crystallized in a monoclinic system at room temperature with the space group of *C*2/*c*. As shown in Fig. 1d, the asymmetric unit of **2Pb** contains four lead(II) ions, eight iodine atoms, and one TETA. Three lead(II) (Pb1, Pb2 and Pb3) ions adopted a geometry of six-coordinated relative regular octahedron (Pb–I: 3.0070 (14) Å–3.3768 (14) Å and I–Pb–I: 85.62 (3)°–178.11 (4)°). The Pb–I bond lengths are closer to the sum of the ionic radii of iodide and lead(II) (ri = 2.2 + 1.03 = 3.23 Å) rather than to that of their covalent radii (re = 1.39 + 1.48 = 2.87 Å), proving that these bonds are ionic in nature. However, the Pb4 ion was coordinated with four nitrogen atoms of the bent TETA (Pb–N: 2.505 (15)–2.596 (19) Å), and two iodine atoms to form $[PbN_4I_2]$ octahedron (Fig. 1e and f). The coordination modes of **2Pb** are quite similar to that of **1Pb**. However, the difference between **1Pb** and **2Pb** was that the Pb–I distance and I–Pb–I angle in the **2Pb** complex were slightly broader than those in **1Pb**, indicating that **2Pb** was a bit distorted from **1Pb**. As shown with **1Pb**, the $[Pb(TETA)]^{2+}$ units in **2Pb** shared two iodine atoms with $[Pb_3I_8]^{2-}$ units to connect them into a 2D network.

TETA showed a regular configuration with normal values of C–C and C–N bond lengths varying from 1.41 (3) Å to 1.55 (3) Å, whereas C–C–C, C–N–C and C–C–N angles ranged between 107.7 (19)° and 117.2 (17)° (see Tables S2 and S3, ESI†). Moreover, **1Pb** and **2Pb** exhibited several intermolecular hydrogen bonding interactions between the cationic and $[Pb_2I_6]^{2-}$ or $[Pb_3I_8]^{2-}$ anions of the type N–H···I and C–H···I listed in Tables S4 and S5 in ESI.† The XRD powder spectra of **1Pb** and **2Pb** are given in Fig. S1, ESI.† It can be seen that PXRD patterns of these two materials matched perfectly well with the simulated results from the single crystal structure, which indicated the high purity of **1Pb** and **2Pb** powder samples.

To analyse and obtain additional information about intermolecular interactions within the crystal structure of **1Pb** and **2Pb**, molecular Hirshfeld surface (MHS) calculations were performed using the crystal explorer 3.1 program. The blue, red and white areas in the MHS represent the largest, shortest and equal to van der Waals separations, respectively (Fig. S2, ESI†). It can be seen from Fig. S3a and c in ESI† that 2D finger

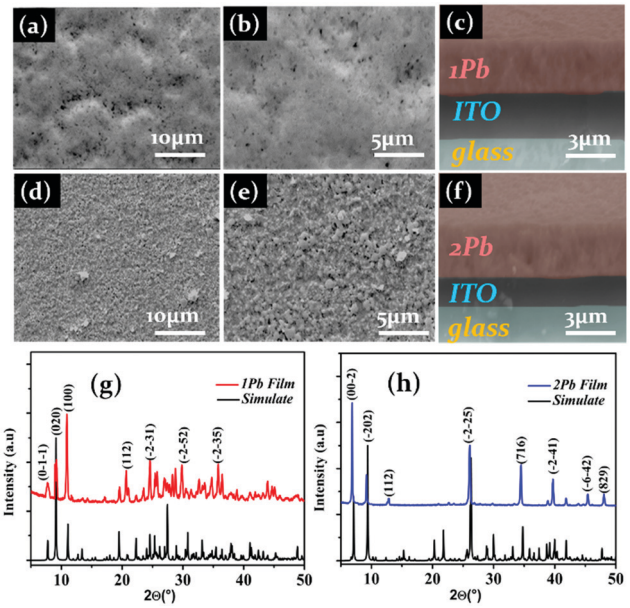

Fig. 2 (a, b) Topographical SEM images of the thin film made from **1Pb**. (c) Cross-sectional SEM image of the thin film made from **1Pb**. (d, e) Topographical SEM images of the thin film made from **2Pb**. (f) Cross-sectional SEM image of thin film made from **2Pb**. (g) XRD patterns of the thin film made from **1Pb**. (h) XRD patterns of the thin film made from **2Pb**.

print maps of **1Pb** and **2Pb** provide quantitative contribution of the intermolecular interaction. Two remarkable spikes presented the most abundant interaction of **1Pb** and **2Pb**, which were from H···I and Pb···I, consistent with the red area in the MHS. It was very clear that hydrogen bonds played an important role in crystal stabilization. These results are also confirmed by single crystal analysis (Tables S4 and S5, ESI†). Other intercontacts present less to MHS were also calculated, such as H···H and I···I (Fig. S3b and d, ESI†).

Significantly, **1Pb** and **2Pb** are highly soluble in dimethylformamide (DMF), and 1 ml DMF can dissolve 0.2 g of each compound (**1Pb** or **2Pb**). Using the one step spin coating technique, we dissolved 20 mg of **1Pb** and **2Pb** single crystals in 1 ml DMF, and then cooled at ambient temperature (More details can be found in the ESI†). Smooth, high coverage, less pin hole films of **1Pb** and **2Pb** readily formed (Fig. 2). **1Pb** and **2Pb** had small grain sizes of 750 nm and 900 nm, respectively ((Fig. 2a and b) and Fig. 2d and e). As shown in Fig. 2c and f, the cross-section images reveal that **1Pb** and **2Pb** have grain thicknesses of 3 μm and 3.1 μm, respectively. XRD patterns of **1Pb** and **2Pb** films match very well with the simulated ones, which indicated their high purity (Fig. 2g and h).

Based on the Kubelka–Munk function,[35] $(F(R) = \alpha/S = (1-R)^2/(2R)$, where R is the reflectance, α is the absorption coefficient, S is the scattering coefficient), the diffuse reflectance spectrum was converted to an absorbance spectrum to understand the semiconducting performance of **1Pb** and **2Pb**. As shown in Fig. 3a, the optical band edges of **1Pb** and **2Pb** were determined to be 2.28 eV and 2.02 eV, respectively. These results are consistent with their colors, and are very similar to other lead iodide hybrid compounds.[36,37] Based on the intercepts of the

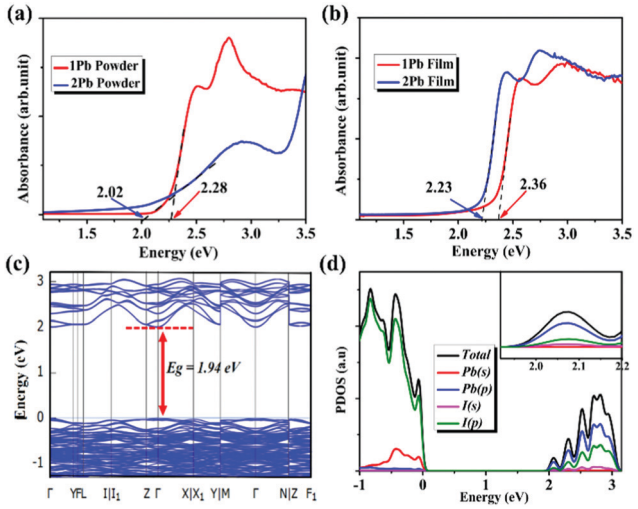

Fig. 3 (a) Absorption spectra for the powder **1Pb** and **2Pb**. (b) Absorption spectra for thin film **1Pb** and **2Pb**. (c) DFT calculations predicted the band structure for **2Pb** with SOC effect included. (d) Simulated orbital resolved partial density of states (PDOS) for **2Pb**.

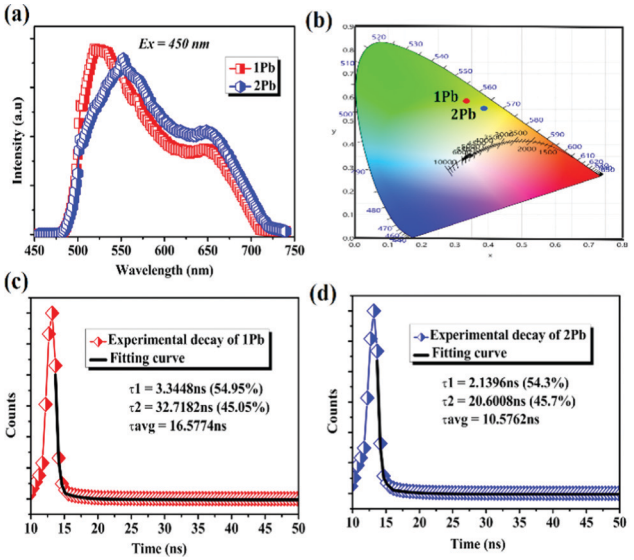

Fig. 4 (a) PL emission spectrum at room temperature for **1Pb** and **2Pb**. (b) CIE chromaticity coordinates for **1Pb** and **2Pb**. (c) Time-resolved decay curve for 645 nm emission at room temperature for **1Pb**. (d) Time-resolved decay curve for 645 nm emission at room temperature for **2Pb**.

curves of $(F(RN)h\nu)^{1/n}$ ($n = 2$ or $n = 1$) *versus* the energy according to the τ_{auc} equation, bandgap energies were estimated to be 2.31 eV (indirect) and 2.20 eV (direct) for **1Pb** and 1.86 eV (indirect) and 2.08 eV (direct), respectively, for **2Pb** (Fig. S4, ESI†). These bandgap values could be considered within the range of a typical semiconductor compound and can be used as the absorber for tandem solar cells when these two materials are coupled with silicon.[38] Interestingly, optical absorption spectra were performed on films of **1Pb** and **2Pb**, respectively, and both are similar for those of powder samples (Fig. 3b).

To get an insight into the electronic properties of these two compounds, DFT calculations of **1Pb** and **2Pb** were performed. After including spin orbital coupling (SOC) effects, GGA-PBE functional predicts that the valence band maximum (VBM) and conduction band minimum (CBM) are both located at the same k points (Γ for **1Pb** and C for **2Pb**), indicating that **1Pb** and **2Pb** are semiconductors with direct bandgaps (Fig. 3c and Fig. S5a, ESI†). In addition, the predicted energy bandgaps are 2.12 eV and 1.94 eV for **1Pb** and **2Pb**, respectively, which are close to experimental results. Without SOC effect, the larger bandgaps of 2.72 eV for **1Pb** and 2.24 eV for **2Pb** will be predicted (Fig. S5b and S6a, ESI†). Based on the partial density of states, we will further analyze the orbital nature for electronic states around VBM and CBM. The top of valence bands was mainly contributed by hybridized I-5p and Pb-6s orbitals, while the bottom of conduction bands had dominant Pb/I-5p orbital characters for both two compounds (Fig. 3d, Fig. S5 (c–f) and S6 (b–d), ESI†). These results clearly indicated that optical excitations within **1Pb** and **2Pb** are mainly determined by the hybridized Pb and I orbitals from the inorganic framework.

The photoluminescence properties of **1Pb** and **2Pb** lead iodide hybrid compounds were studied at room temperature using steady state and time-resolved emission spectroscopy. Upon excitation of 450 nm, both compounds exhibited two band emissions, which generally matched very well with the two slopes from the absorption spectra. Indeed, **1Pb** and **2Pb** display two broadband emissions with the highest bands at 519 nm for **1Pb** and 550 nm for **2Pb**, and another two weak emissions present in the range of 600–720 nm can be tentatively assigned to lead halide-centered transitions within the inorganic group, as suggested by band structure calculations, and observed recently in other reported iodoplumbate organic–inorganic based hybrid materials (Fig. 4a).[39–41] Thus, the broad photoluminescence mainly originated from the inorganic component. We should note that similar emission bands between **1Pb** and **2Pb** indicate the same radiative recombination route. In addition, the combination of the two emission bands gave rise to the CIE 1931 chromaticity coordinates of (0.39, 0.56) for **1Pb** with CCT of 3780 K and of (0.43, 0.53) for **2Pb** with CCT of 3825 K. Both compounds exhibited yellow green emission (Fig. 4b). Moreover, the PLQY of **1Pb** and **2Pb** was measured to be 1% and 1.12%, respectively, which were comparable to those of previous reported 2D hybrid lead materials, such as 0.5% for (N–MEDA)PbI_4 and ~1% for $(C_6H_5C_2H_4NH_3)_2PbCl_4$.[42,43]

Using a fitting with a double-exponential function $I(t) = A_1\exp(-t/\tau_1) + A_2\exp(-t/\tau_2)$, the decay life times of **1Pb** and **2Pb** have been calculated (Fig. 4c and d). Interestingly, the average life time for **1Pb** was 16.57 ns and for **2Pb** was 10.57 ns, which were longer than that of other reported 2D lead hybrid compounds (Table S6, ESI†). The photoluminescence properties for both compounds are summarized in Table 1.

Table 1 Summary of the photophysical properties of **1Pb** and **2Pb**

Compds	λ_{ex} (nm)	λ_{em} (nm)	CIE	τ (ns)
1Pb	450	518/645	(0.39, 0.56)	16.57
2Pb	450	550/645	(0.43, 0.53)	10.57

The photoconductivity of **1Pb** and **2Pb** was studied using film samples as the active layer under the illumination from a 350 W Xenon lamp irradiation at 0.7 V bias (more details can be found in the ESI†). As shown in Fig. 5a and c, both materials exhibited a strong photoresponse in that the photocurrent for **1Pb** enhanced from 20 to 636 nm cm^{-2}, and increased for **2Pb** from 42 to 780 nm cm^{-2}. Those values are higher than that of bismuth halide organic–inorganic materials and comparable to that of lead-based hybrids. However, they were lower than that of 3D $MAPbI_3$ and those of inorganic systems.[39,40,44–48] To the best of our knowledge, **1Pb** and **2Pb** had among the highest current obtained in 2D lead iodide hybrid materials under low voltages. We need to mention that the order of photocurrent for these two compounds was well coherent with their optical bandgaps, which signalized that a small bandgap may be better to generate and separate a photoinduced electron/hole.[37,49]

Fig. 5b and d show that these devices exhibited a broadband, repeatable and periodical switching (on/off) of the light, which means that **1Pb** and **2Pb** exhibited an obvious photocurrent reproducibility and high stability. Moreover, the photoresponsivity (R) (it is an important figure of merit to represent the sensitivity of the photodetector to the light signal) was calculated to be 7.04 μA W^{-1} and 8.57 μA W^{-1} for **1Pb** and **2Pb**, respectively.

Other important parameters of photodetector devices, such as detectivity (D^*) and external quantum efficiency (EQE), were also determined. A comparative table between **1Pb** and **2Pb** with other general materials are illustrated in Table S7 in the ESI.† The responsivity, detectivity and external quantum efficiency are obtained using the following equations:

$$R = \frac{I_{light} - I_{dark}}{P_0 S} \quad (1)$$

$$D^* = RS^{\frac{1}{2}}/(2eI_d)^{\frac{1}{2}} \quad (2)$$

$$EQE = R \times \frac{12408}{\lambda} \quad (3)$$

where I_{light} is the photocurrent, I_{dark} is the dark current, P_0 is the intensity of light, S is the area of the device, e is the electronic charge and λ is the wavelength of irradiation.

Moreover, we studied the stability of both **1Pb** and **2Pb** towards moisture, light and heat. The as-prepared films of **1Pb** and **2Pb** were stored in the dark at 55% relative humidity for 7 days. The XRD patterns of the film samples of **1Pb** and **2Pb** remained almost the same as those of the freshly prepared sample (see Fig. S1, ESI†) and showed no evidence of peak related to material degradation. However, we noted a decrease in the diffraction peak intensity of **1Pb** and **2Pb** within 7 days (Fig. S7, ESI†). To explore the UV aging effect, we exposed **1Pb** and **2Pb** films to UV light for 24 h at room temperature. No obvious change has been observed for the XRD patterns compared to the simulated ones (Fig. S7, ESI†). Moreover, to evaluate the thermal stability of **1Pb** and **2Pb**, thermogravimetric analyses (TGA) were conducted from 30 °C to 600 °C under nitrogen atmosphere (Fig. S8, ESI†). It can be seen from the TGA curves that the two compounds are stable up to 225 °C. Hence, **1Pb** and **2Pb** showed high stability towards moisture, light and heat.

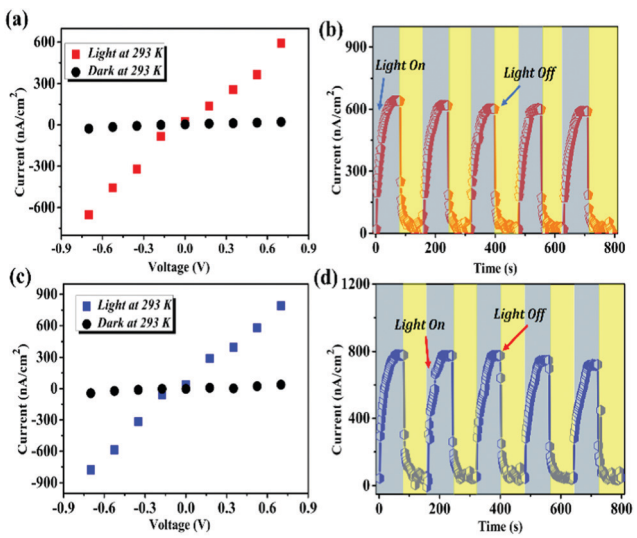

Fig. 5 (a, c) I–V plots for dark and light current of **1Pb** (a) and **2Pb** (c) measured at 298 K. (b, d) I–t plots of several irradiation cycles of **1Pb** (b) and **2Pb** (d).

Conclusions

In summary, two new 2D organic–inorganic hybrid lead iodide using a tetradentate ligand were successfully synthesized and fully characterized. Both compounds exhibited an excellent semiconductor property and showed broadband yellow-green emission. Interestingly, **1Pb** and **2Pb** showed high stability and exhibited a strong photocurrent response at 0.7 V. In addition, **1Pb** and **2Pb** were processed into high coverage films through the one-spin coating method. Thus, this study showed two new broadband 2D lead iodide hybrid materials with potential for light detection applications.

Author contributions

M. S. Lassoued, Y.-C. Pang and Q.-W. Li conducted the syntheses, crystallography and photoluminescence. The *ab initio* calculations were performed by X. Ding, G. Gou and J. Li. The photoresponse measurements were performed by Z. Yin, B. Jiao and H. Dong; G. Zhou, S. Ding, Z. Zhang and Z. Wu drew the pictures and wrote the manuscript; Y.-Z. Zheng supervised the whole project. All authors read and approved the manuscript before submission.

Conflicts of interest

There are no conflicts to declare.

Acknowledgements

This work was supported by the Natural Science Foundation of China (no. 21971203 and 21773130), the State Key Laboratory for Mechanical Behavior of Materials (20182006), the Key Laboratory Construction Program of Xi'an Municipal Bureau of Science and Technology (201805056ZD7CG40), the China Postdoctoral Science Foundation (2018M631138), the Shaanxi Postdoctoral Science Foundation (2018), the Cyrus Chung Ying Tang Foundation and the Fundamental Research Funds for Central Universities, Key Scientific and Technological Innovation Team of Shaanxi Province (2020TD-001).

References

1 A. Kojima, K. Teshima, Y. Shirai and T. Miyasaka, Organometal halide perovskites as visible-light sensitizers for photovoltaic cells, *J. Am. Chem. Soc.*, 2009, **131**, 6050–6051.
2 M. M. Lee, J. Teuscher, T. Miyasaka, T. N. Murakami and H. J. Snaith, Efficient hybrid solar cells based on meso-superstructured organometal halide perovskites, *Science*, 2012, **338**, 643–647.
3 J. Burschka, N. Pellet, S.-J. Moon, R. Humphry-Baker, P. Gao, M. K. Nazeeruddin and M. Graetzel, Sequential deposition as a route to high-performance perovskite-sensitized solar cells, *Nature*, 2013, **499**, 316–319.
4 X. Li, D. Bi, C. Yi, J.-D. Decoppet, J. Luo, S. M. Zakeeruddin, A. Hagfeldt and M. Gratzel, A vacuum flash–assisted solution process for high-efficiency large-area perovskite solar cells, *Science*, 2016, **353**, 58–62.
5 W. S. Yang, J. H. Noh, N. J. Jeon, Y. C. Kim, S. Ryu, J. Seo and S. I. Seok, High-performance photovoltaic perovskite layers fabricated through intramolecular exchange, *Science*, 2015, **348**, 1234–1237.
6 E. L. Unger, E. T. Hoke, C. D. Bailie, W. H. Nguyen, A. R. Bowring, T. Heumueller, M. G. Christoforo and M. D. McGehee, Hysteresis and transient behavior in current–voltage measurements of hybrid-perovskite absorber solar cells, *Energy Environ. Sci.*, 2014, **7**, 3690–3698.
7 The National Renewable Energy Laboratory (NREL) Best Research-Cell Record Efficiencies, Best Research-Cell Efficiency Chart (nrel.gov).
8 L. Martiradonna, Entropy in halide perovskites, *Nat. Mater.*, 2018, **17**, 377–379.
9 L. Etgar, The merit of perovskite's dimensionality; can this replace the 3D halide perovskite?, *Energy Environ. Sci.*, 2018, **11**, 234–242.
10 B. W. Park and S. I. Seok, Intrinsic Instability of Inorganic–Organic Hybrid Halide Perovskite, Materials, *Adv. Mater.*, 2019, **3**, 1805337.
11 M. S. Lassoued, L.-Y. Bi, Z. Wu, G. Zhou and Y.-Z. Zheng, Piperidine-induced Switching of the direct band gaps of Ag(I)/Bi(III) bimetallic iodide double perovskites, *J. Mater. Chem. C*, 2020, **8**, 5349–5354.
12 M. S. Lassoued, L.-Y. Bi, Z. Wu, G. Zhou and Y.-Z. Zheng, Two-dimensional semiconducting Cs(i)/Bi(iii) bimetallic iodide hybrids for light detection, *Mater. Chem. Front.*, 2021, **5**, 973–978.
13 L.-Y. Bi, Y.-Q. Hu, M.-Q. Li, T.-L. Hu, H.-L. Zhang, X.-T. Yin, W.-X. Que, M. S. Lassoued and Y.-Z. Zheng, Two-dimensional lead-free iodide-based hybrid double perovskites: crystal growth, thin-film preparation and photocurrent responses, *J. Mater. Chem. A*, 2019, **7**, 19662–19667.
14 I. C. Smith, E. T. Hoke, D. Solis-Ibarra, M. D. McGehee and H. I. Karunadasa, A Layered Hybrid Perovskite Solar-Cell Absorber with Enhanced Moisture Stability, *Angew. Chem., Int. Ed.*, 2014, **53**(42), 11232–11235.
15 D. H. Cao, C. C. Stoumpos, O. K. Farha, J. T. Hupp and M. G. Kanatzidis, 2D Homologous Perovskites as Light-Absorbing Materials for Solar Cell Applications, *J. Am. Chem. Soc.*, 2015, **137**(24), 7843–7850.
16 H. Tsai, W. Nie, J.-C. Blancon, C. C. Stoumpos, R. Asadpour, B. Harutyunyan, A. J. Neukirch, R. Verduzco, J. J. Crochet, S. Tretiak, L. Pedesseau, J. Even, M. A. Alam, G. Gupta, J. Lou, P. M. Ajayan, M. J. Bedzyk, M. G. Kanatzidis and A. D. Mohite, High efficiency two-dimensional Ruddlesden–Popper perovskite solar cells, *Nature*, 2016, **536**(7616), 312–316.
17 M. Leng, Z. Chen, Y. Yang, Z. Li, K. Zeng, K. Li, G. Niu, Y. He, Q. Zhou and J. Tang, Lead-Free, Blue Emitting Bismuth Halide Perovskite Quantum Dots, *Angew. Chem., Int. Ed.*, 2016, **55**, 15012–15016.
18 D. B. Mitzi, Organic–Inorganic Perovskites Containing Trivalent Metal Halide Layers: The Templating Influence of the Organic Cation Layer, *Inorg. Chem.*, 2000, **39**, 6107–6113.
19 N. Mercier, S. Poiroux, A. Riou and P. Batail, Unique hydrogen bonding correlating with a reduced band gap and phase transition in the hybrid perovskites $(HO(CH_2)_2NH_3)_2PbX_4$ (X = I, Br), *Inorg. Chem.*, 2004, **43**, 8361–8366.
20 D. G. Billing and A. Lemmerer, Inorganic–organic hybrid materials incorporating primary cyclic ammonium cations: The lead iodide series, *CrystEngComm*, 2007, **9**, 236–244.
21 H. Krautscheid and F. Vielsack, Synthese und Kristallstrukturen kettenförmiger und netzartiger Iodoplumbate, *Z. Anorg. Allg. Chem.*, 1997, **623**, 259–263.
22 H. Krautscheid and F. Vielsack, Discrete and polymeric iodoplumbates with Pb_3I_{10} building blocks: $[Pb_3I_{10}]^{4-}$, $[Pb_7I_{22}]^{8-}$, $[Pb_{10}I_{28}]^{8-}$, $1\infty[Pb_3I_{10}]^{4-}$ and $2\infty[Pb_7I_{18}]^{4-}$, *J. Chem. Soc., Dalton Trans.*, 1999, 2731–2735.
23 H. Krautscheid, F. Vielsack and N. Klaassen, Polymere Iodoplumbate – Synthese und Kristallstrukturen von $(Pr_3N–C_2H_4–NPr_3)[Pb_6I_{14}(dmf)_2]$ 4 DMF, $(Pr_3N–C_2H_4–NPr_3)[Pb(dmf)_6][Pb_5I_{14}]$ DMF und $(Me_3N–C_2H_4–NMe_3)_2[Pb_2I_7]$I, *Z. Anorg. Allg. Chem.*, 1998, **624**, 807–812.
24 Y. Gao, E. Shi, S. Deng, S. B. Shiring, J. M. Snaider, C. Liang, B. Yuan, R. Song, S. M. Janke, A. L-Peláez, P. Yoo, M. Zeller, B. W. Boudouris, P. Liao, C. Zhu, V. Blum, Y. Yu, B. M. Savoie, L. Huang and L. Dou, Molecular engineering of organic-inorganic hybrid perovskites quantum wells, *Nat. Chem.*, 2019, **11**, 1151–1157.
25 Y. Gao, Z. Wei, S.-N. Hsu, B. W. Boudouris and L. Dou, Two-dimensional halide perovskites featuring semiconducting

organic building blocks, *Mater. Chem. Front.*, 2020, **4**, 3400–3418.

26 S. Ahmad, P. Fu, S. Yu, Q. Yang, X. Liu, X. Wang, X. Wang, X. Guo and C. Li, Dion-Jacobson Phase 2D Layered Perovskites for Solar Cells with Ultrahigh Stability, *Joule*, 2018, **3**, 794–806.

27 C. Deng, G. Zhou, D. Chen, J. Zhao, Y. Wang and Q. Liu, Broadband Photoluminescence in 2D Organic−Inorganic Hybrid Perovskites: $(C_7H_{18}N_2)PbBr_4$ and $(C_9H_{22}N_2)PbBr_4$, *The*, *J. Phys. Chem. Lett.*, 2020, **11**(8), 2934–2940.

28 Y. Li, C. Ji, L. Li, S. Wang, S. Han, Y. Peng, S. Zhang and J. Luo, γ-Methoxy propyl amine)2PbBr4: a novel two-dimensional halide hybrid perovskite with efficient bluish white-light emission, *Inorg. Chem. Front.*, 2021, **8**, 2119–2124.

29 C.-Q. Jing, J. Wang, H.-F. Zhao, W.-X. Chu, Y. Yuan, Z. Wang, M.-F. Han, T. Xu, J.-Q. Zhao and X.-W. Lei, Improving Broadband White-Light Emission Performances of 2D Perovskites by Subtly Regulating Organic Cations, *Chem. – Eur. J.*, 2020, **26**, 10307–10313.

30 C. Xue, S. Wang, W.-L. Liu and X.-M. Ren, Two-Step Structure Phase Transition, Dielectric Anomalies, and Thermochromic Luminescence Behavior in a Direct Band Gap 2D Corrugated Layer Lead Chloride Hybrid of $[(CH_3)_4N]_4Pb_3Cl_{10}$, *Chem. – Eur. J.*, 2019, **25**, 5280–5287.

31 C. Ji, S. Wang, L. Li, Z. Sun and M. Hong, The First 2D Hybrid Perovskite Ferroelectric Showing Broadband White-Light Emission with High Color Rendering Index, *Adv. Funct. Mater.*, 2019, **29**, 1805038.

32 P. Cai, Y. Huang and H. J. Seo, Anti-Stokes Ultraviolet Luminescence and Exciton Detrapping in the Two-Dimensional Perovskite $(C_6H_5C_2H_4NH_3)_2PbCl_4$, *J. Phys. Chem. Lett.*, 2019, **10**(14), 4095–4102.

33 D. Fu, J. Yuan, S. Wu, Y. Yao, X. Zhang and X.-M. Zhang, A two-dimensional bilayered Dion–Jacobson-type perovskite hybrid with a narrow bandgap for broadband photodetection, *Inorg. Chem. Front.*, 2020, **7**, 1394–1399.

34 J. Zhou, Y. Chu and J. Huang, Photodetectors Based on Two-Dimensional Layer-Structured Hybrid Lead Iodide Perovskite Semiconductors, *ACS Appl. Mater. Interfaces*, 2016, **8**, 25660–25666.

35 J. Tauc, Absorption edge and internal electric fields in amorphous semiconductors, *Mater. Res. Bull.*, 1970, **5**, 721–729.

36 C.-Y. Yue, H.-X. Sun, Q.-X. Liu, X.-M. Wang, Z.-S. Yuan, J. Wang, J.-H. Wu, B. Hu and X.-W. Lei, Organic cation directed hybrid lead halides of zero-dimensional to two-dimensional structures with tunable photoluminescence properties, *Inorg. Chem. Front.*, 2019, **6**, 2709–2717.

37 B. Zhang, H.-Y. Sun, J. Li, Y.-R. Xu, Y.-P. Xu, X. Yang and G.-D. Zou, Hybrid iodoplumbates with metal complexes: syntheses, crystal structures, band gaps and photoelectric properties, *Dalton Trans.*, 2020, **49**, 1803–1810.

38 R. Sheng, A. W. Ho-Baillie, S. Huang, M. Keevers, X. Hao, L. Jiang, Y. B. Cheng and M. A. Green, Four-Terminal Tandem Solar Cells Using $CH_3NH_3PbBr_3$ by Spectrum Splitting, *J. Phys. Chem. Lett.*, 2015, **6**, 3931–3934.

39 T.-t. Zhang, X. Liu, J. Zhou and J.-t. Liu, Two Organic Hybrid Iodoplumbates Directed by a Bifunctional Bis(pyrazinyl) triazole, *Inorg. Chem.*, 2021, **60**, 5362–5366.

40 Y. He, Y.-R. Huang, Y.-L. Li, H.-H. Li, Z.-R. Chen and R. Jiang, Encapsulating Halometallates into 3-D Lanthanide-Viologen Frameworks: Controllable Emissions, Reversible Thermochromism, Photocurrent Responses, and Electrical Bistability Behaviors, *Inorg. Chem.*, 2019, **58**(20), 13862–13880.

41 X.-L. Lin, B. Chen, Y.-R. Huang, K.-Y. Song, P.-K. Zhou, L.-L. Zong, H.-H. Li, Z.-R. Chen and R. Jiang, Achievement of intrinsic white light emission by hybridization-deformable haloplumbates with rigid luminescent naphthalene motifs, *Inorg. Chem. Front.*, 2020, **7**, 4477–4487.

42 E. R. Dohner, A. Jaffe, L. R. Bradshaw and H. I. Karunadasa, Intrinsic white-light emission from layered hybrid perovskites, *J. Am. Chem. Soc.*, 2014, **136**, 13154–13157.

43 C. Ji, S. Wang, L. Li, Z. Sun, M. Hong and J. Luo, The first 2D hybrid perovskite ferroelectric showing broadband white–light emission with high color rendering index, *Adv. Funct. Mater.*, 2018, **29**, 1805038.

44 J. K. Pious, A. Katre, C. Muthu, S. Chakraborty, S. Krishna and C. Vijayakumar, Zero-Dimensional Lead-Free Hybrid Perovskite-like Material with a Quantum-Well Structure, *Chem. Mater.*, 2019, **31**, 1941–1945.

45 N. Chen, Y. Gao, Y. Tian, B. Wu, D. Jia and S. Zhao, One-dimensional polymeric iodoplumbate hybrids with lanthanide complex cations: syntheses, crystal structures, and photoelectric and photocatalytic properties, *New J. Chem.*, 2020, **44**, 19166–19173.

46 A. Dey, J. Ye, A. De, E. Debroye, S. K. Ha, E. Bladt, A. S. Kshirsagar, Z. Wang, J. Yin, Y. Wang, L. N. Quan, F. Yan, M. Gao, X. Li, J. Shamsi, T. Debnath, M. Cao, M. A. Scheel, S. Kumar, J. A. Steele, M. Gerhard, L. Chouhan, K. Xu, X.-g. Wu, Y. Li, Y. Zhang, A. Dutta, C. Han, I. Vincon, A. L. Rogach, A. Nag, A. Samanta, B. A. Korgel, C.-J. Shih, D. R. Gamelin, D. H. Son, H. Zeng, H. Zhong, H. Sun, H. V. Demir, I. G. Scheblykin, I. M-Seró, J. K. Stolarczyk, J. Z. Zhang, J. Feldmann, J. Hofkens, J. M. Luther, J. P-Prieto, L. Li, L. Manna, M. I. Bodnarchuk, M. V. Kovalenko, M. B. J. Roeffaers, N. Pradhan, O. F. Mohammed, O. M. Bakr, P. Yang, P. M-Buschbaum, P. V. Kamat, Q. Bao, Q. Zhang, R. Krahne, R. E. Galian, S. D. Stranks, S. Bals, V. Biju, W. A. Tisdale, Y. Yan, R. L. Z. Hoye and L. Polavarapu, State of the Art and Prospects for Halide Perovskite Nanocrystals, *ACS Nano*, 2021, **15**, 10775–10981.

47 Y. Tang, M. Liang, Bi. Chang, H. Sun, K. Zheng, T. Pulleritsd and Q. Chi, Lead-free double halide perovskite Cs_3BiBr_6 with well-defined crystal structure and high thermal stability for optoelectronics, *J. Mater. Chem. C*, 2019, **7**, 3369–3374.

48 Y. Dang, G. Tong, W. Song, Z. Liu, L. Qiu, L. K. Ono and Y. Qi, Interface engineering strategies towards $Cs_2AgBiBr_6$ single-crystalline photodetectors with good Ohmic contact behaviours, *J. Mater. Chem. C*, 2020, **8**, 276–284.

49 M.-Q. Li, Y.-Q. Hu, L.-Y. Bi, H.-L. Zhang, Y. Wang and Y.-Z. Zheng, Structure Tunable Organic−Inorganic Bismuth Halides for an Enhanced Two-Dimensional Lead-Free Light-Harvesting Material, *Chem. Mater.*, 2017, **29**(13), 5463–5467.